A compact rotary magnetic tweezers device for dynamic material analysis

John P. Berezney¹ and Megan T. Valentine¹
Mechanical Engineering Department, University of California, Santa Barbara, California 93106, USA^{a)}

(*The author to whom correspondence may be addressed: valentine@engineering.ucsb.edu)

(Dated: 15 July 2022)

Here we present a new, compact magnetic tweezers design that enables precise application of a wide range of dynamic forces to soft materials without the need to raise or lower the magnet height above the sample. This is achieved through the controlled rotation of the permanent magnet array with respect to the fixed symmetry axis defined by a custom-built iron yoke. These design improvements increase the portability of the device and can be implemented within existing microscope setups without the need for extensive modification of the sample holders or light path. This device is particularly well-suited to active microrheology measurements using either creep analysis, in which a step force is applied to a micron-sized magnetic particle that is embedded in a complex fluid, or oscillatory microrheology, in which the particle is driven with a periodic waveform of controlled amplitude and frequency. In both cases, the motions of the particle are measured and analyzed to determine the local dynamic mechanical properties of the material.

Keywords: rheology, microrheology, tweezers, viscoelasticity, single-molecule

I. INTRODUCTION

Microrheology devices measure the behavior of complex viscoelastic materials at small length scales over which inhomogeneities and microstructures strongly contribute to material response. Such techniques have been used to understand the complex physics which governs the behavior of soft structured materials, such as DNA solutions, carbon nanotube suspensions, liquid crystals, cytoskeletal networks and living cells $^{1-6}$. Common experimental approaches include the analysis of the thermal motions of embedded particles (called "passive" microrheology) or the analysis of the driven motions of particles using optical or magnetic tweezers (called "active" microrheology) 7 . Of these, magnetic tweezers can apply the highest forces and exhibit the largest dynamic force range, thus enabling measurement of the broadest range of materials, with moduli as high as $\approx 1~\rm kPa$ $^{8.9}$.

Such particle-based microrheology methods typically leverage optical microscopy to observe and record particle motion, and are thus well-suited for combination with other microscopy techniques (e.g. fluorescence microscopy, confocal scanning microscopy, FCS, FRAP) to characterize materials more fully¹⁰. However, such combinations are only possible if the microrheology device can be physically coupled to the microscope of interest. Although simple portable versions of magnetic tweezers devices exist, they typically do not provide large applied forces, can be difficult to calibrate, and it is challenging to dynamically vary the applied force¹¹. By contrast high-force magnetic tweezers are typically built around custom microscope bases, in order to accommodate the custom-built magnet arrays^{12–14}.

To achieve large forces, large magnetic field gradients are required. These have been demonstrated using electromagnetic devices, which allow for rapid changes in field strength by changes in applied current^{6,15,16}. Yet electromagnetic devices have disadvantages: they typically exhibit hysteretic responses and require high-voltage power supplies and computerized feedback control to provide well-controlled forces. Moreover, because of the high currents required, such devices can require active cooling to prevent sample overheating due to Joule heating^{15,17}.

Permanent rare earth magnets, typically formed from an alloy of neodymium, iron, and boron (NdFeB), are an excellent alternative and can provide similar magnetic field gradients, and thus similar forces, at the sample plane. In this case, the magnetic field amplitude and gradient are determined by the specific magnetic material selection and array design and the field values are fixed with respect to the magnet rest frame^{18,19}. The field gradients, and thus forces, can be easily and robustly varied with respect to the specimen plane using motorized stages that change the separation distance between the magnet array and the sample²⁰. Although the use of precision linear stages, rather than current control, significantly simplifies the design, eliminates the possibility of hysteretic responses and removes the need for cooling and complex electronics^{17,21}, it also introduces several implementation challenges, including the disruption of the light path, an inability to apply true step forces due to the finite translation time of the heavy magnets, and noise associated with the motion and settling of the magnet into position. Moreover, such motions can be on the order of centimeters, requiring significant physical space above the specimen plane to accommodate the magnet array, motors, and travel distance. These space requirements limit the broad application of NdFeB-magnet based magnetic tweezers devices in conjunction with commercially-available microscopes. Finally, although it is possible to achieve oscillatory forces with NdFeB-based microrheology devices by translating the magnetic array along the optical axis²², achieving oscillation around zero applied force is challenging, and it is difficult to probe high frequency behavior (>5 Hz) because the motion creates vibrations which propagate through the instrument, causing a deleterious decrease in the signal to noise ratio. Thus, compact devices that allow for faster force-

a) John Berezney's present address is Physics Department, Brandeis University, Waltham, Massachusetts.

switching for creep analysis and oscillatory microrheology are desired.

In this work, we describe a simple, motor-driven NdFeBbased magnetic tweezers instrument which eliminates the need for translational movement of the magnet assembly altogether. This is achieved by the use of a different magnet geometry, in which a diametrically-magnetized cylindrical magnet is rotated in plane with respect to a fixed field-focusing iron yoke. This produces a time-varying magnetic field at the specimen plane. Through use of appropriate calibration and motor control, we demonstrate that it is possible to apply constant applied forces across three decades of force and to produce periodic force waveforms over two decades of frequencies (0.01 Hz to 1 Hz). Additionally, because the device relies on a rotary magnet within a small enclosed magnet assembly, the compact device is effectively static in the experimental setup; this reduces the spatial requirements for implementation and allows incorporation into complicated experimental configurations, while significantly reducing the time to switch the magnet array into different force configurations.

II. DEVICE DESIGN

The key innovation in this design is the use of a diametrically opposed cylindrical magnet (RX04X0DIA, K&J Magnetics) which is oriented with respect to a fixed iron yoke with tips that focus and direct the magnetic field toward the sample (see Fig. 1, inset) ¹⁸. Rotating the cylindrical magnet about its central axis changes its alignment with respect to the focusing yoke and thereby creates a time varying magnetic field at the sample, which varies from zero to about 0.1 T in our design. We used a servo motor (AKM23F, Kollmorgen) to drive this rotation and control the rotation speed. Concomitantly, the magnetic field gradient varies, which provides a time varying applied force on paramagnetic probe beads positioned at the specimen plane.

To demonstrate the full range of capabilities of this device, and enable a broad range of dynamic mechanical measurements of soft materials, the magnet array was then incorporated into a previous magnetic tweezers design²². Imaging was achieved using a custom built inverted microscope in which images are collected by a CCD camera and fed into custom LabVIEW algorithms capable of extracting the three-dimensional movement of multiple probe beads in real time. The magnet assembly was mounted onto a stepper motor driven gantry to control the height of the magnet array above the specimen plan. This gantry was designed to achieve well-controlled, low-noise application of oscillatory force, as previously described²². . We note that linear translation was used here as a convenient means of dynamically changing the applied force range in order to test a wide range of materials and magnetic beads and to fully investigate the instrument performance. However, a linear stage is not required to achieve force modulation through rotation, a key feature of this design. The instrument could be further simplified if rapid force modulation was not required by replacing the rotary motor with a simple manual rotary mount. This would significantly

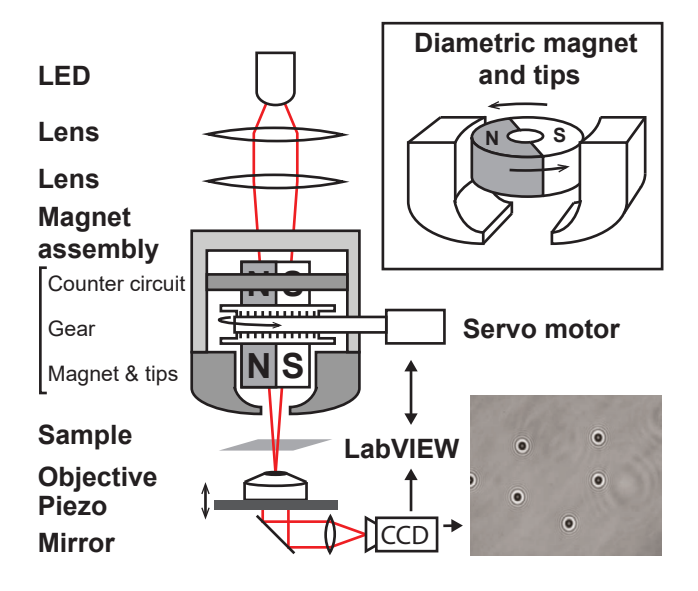


FIG. 1. The device is designed to apply forces to paramagnetic beads using a compact rotating magnet assembly instead of translating magnets over centimeter-scale distances. A hollow core diametric magnet is surrounded by a iron yoke which directs the magnetic field through tips to the sample plane. As the magnets are rotated by a servo motor, the field gradient at the sample plane is changed. The magnet assembly also incorporates a counter circuit which decreases the cogging torque generated by the magnet and iron yoke.

increase the device portability and reduce cost.

Using an F. W. Bell gaussmeter (Model 5170) fixed to the sample holder, we recorded the magnetic field as a function of rotational angle ϕ and separation distance z between the probe and the magnet assembly. We assigned $\phi=0$ to the magnet position where field gradient is maximum. We find that the magnetic field gradient oscillates with the rotational position of the magnet assembly and decreases smoothly with increasing separation distance (Fig. 2). Thus, by continuously rotating the magnet at fixed magnet height, an oscillatory magnetic field gradient may be be applied to the sample plane.

As the cylindrical magnet is rotated, a significant cogging torque is created by the attraction between the iron yoke and the rotating cylindrical magnet, which is a challenge for a compact motor to overcome. To mitigate this effect, we employ a second magnetic circuit to counter the cogging (Fig. 1). A second cylindrical magnet is placed above the active magnet and is surrounded by an iron piece whose shape mimics the yoke but whose orientation is rotated 90°. As the whole magnet spindle assembly rotates, the cogging torques developed by the counter circuit and active magnetic circuit are superimposed and partially cancel, thus significantly reducing the cogging torque the servo motor must overcome to continuously rotate the magnet. Although it may be possible to eliminate cogging with more complex yoke/tip design, we opted for a simpler design and selected a servo motor capable of overcoming the remaining cogging force using active feedback loops.

Realtime control of the Kollmorgen AKM23F servo motor was carried out using a Kollmorgen Single Axis Servo

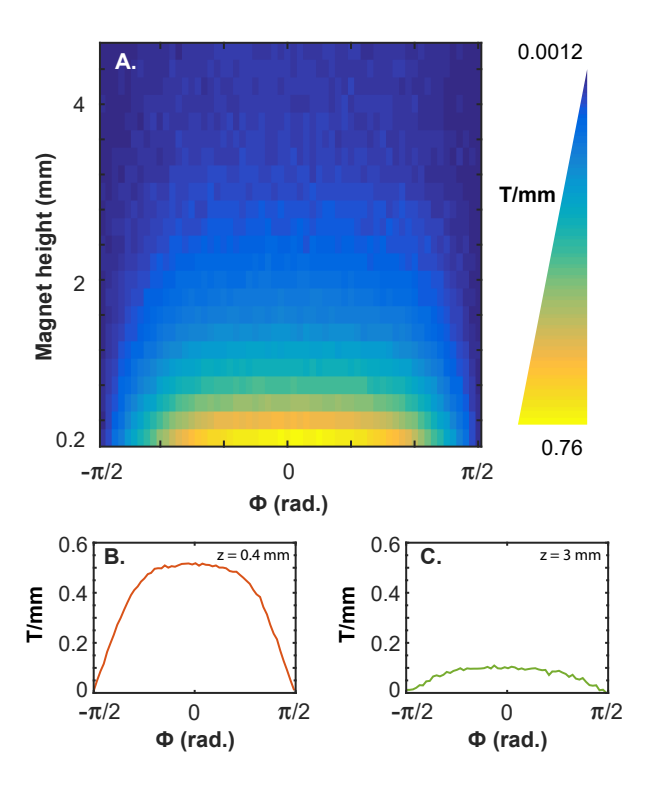


FIG. 2. (A) The gradient of the magnetic field, which determines the applied force on paramagnetic beads, depends on both the rotational magnet position, ϕ , and the height of the magnet above the sample, z. (B) and (C) show line profiles for two particular separation distances, $z=0.4\,\mathrm{mm}$ and $z=3\,\mathrm{mm}$. As the magnets are rotated through ϕ , the field gradient increases from and then decreases to zero. The magnitude of this increase is controlled by the vertical position of the magnet assembly, z.

Drive (AKD-P00606-NBEC-0000), a National Instruments (NI) Servo Drive Interface (NI 9516) and an NI CompactRIO Controller (CRIO-9030). This hardware configuration allows users to employ high-level commands within the NI Lab-VIEW SoftMotion software module to control motors and drives. We used a simple LabVIEW module to command the motor drive to maintain constant velocity on the servo motor. This is made possible through PID control loops enacted within the hardware which respond to changes in the speed at the microsecond timescale.

III. OPERATION AND EXPERIMENTAL VALIDATION

This oscillatory magnetic field gradient produces an oscillatory force on superparamagnetic particles given by $\vec{F} = \vec{\nabla}(\vec{m} \cdot \vec{B})$, where m is the magnetic moment of the particle and B is the magnetic field. In our design, the magnetic field gradient is overwhelmingly in the z direction, which is along the optical axis and orthogonal to the sample plane, and the small superparamagnetic particles employed quickly become saturated under the relatively large magnetic fields present in our experiments²³. Therefore, the force experienced by the par-

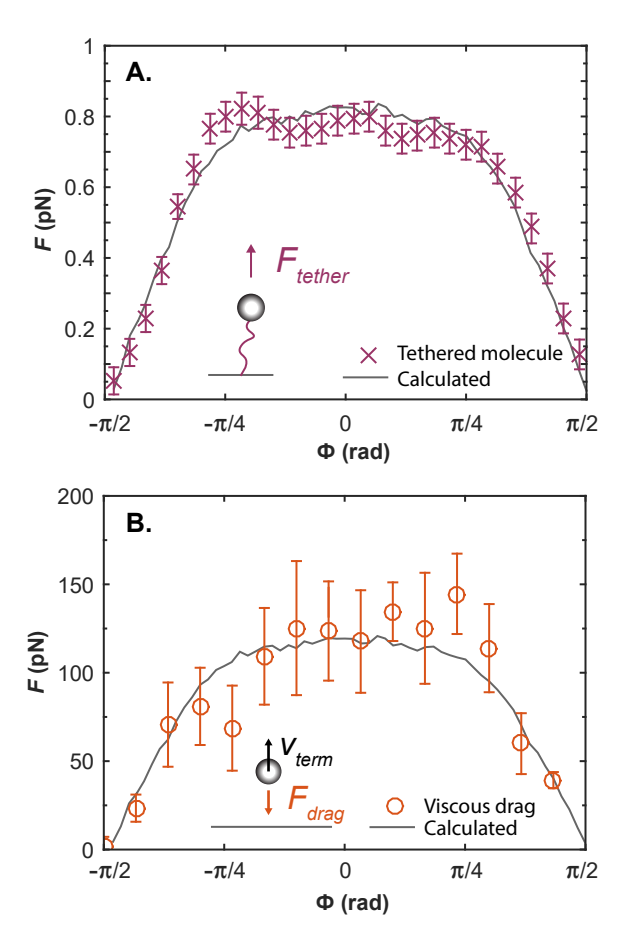


FIG. 3. Various configurations of bead size and magnet separation height allow a large range of applied forces. This range can be estimated accurately by directly measuring the magnetic field and using known magnetic properties of paramagnetic beads. We confirm there is strong agreement between the force values measured by multiple methods and the forces calculated from the measured magnetic field. (A) Forces measured through the motion of a single-molecule tethered particle agree with forces measured from the gradient in the magnetic field. (B) Much higher forces measured through the the drag force on colloidal beads are in agreement with the forces measured through the gradient in the magnetic field.

ticles is well-approximated by $F_z = m_{sat} \frac{\partial B}{\partial z}$, where m_{sat} represents the saturated magnetic moment of the colloidal particle. Moreover, in cases where m_{sat} is known, as is the case for many commercially produced magnetic beads, it is possible to calculate the force experienced by the beads from direct measurements of the magnetic field²³. In this work, we use polystyrene beads with diameters ranging from about 1 μ m to 22 μ m into which a paramagnetic material is embedded, allowing the applied force to vary from about 0.1 pN to 1000 pN. Two modes of operation are explored: rapid force switching via the application of step force profiles, and oscillatory force profiles via the continuous rotation of the magnet array.

To investigate and validate the dynamic force capabilities of the device, the motion of these beads in the sample is captured with a CCD camera and analyzed using particle tracking algorithms to give three dimensional trajectories, as previous described ^{12,21,24}. Briefly, to track the 2D motions within the image plane, a line is drawn through the bead center and the line intensity is calculated for every frame in both the x and y directions. A convolution between the line intensity of a given frame and the line intensity from the previous frame is performed. The x- and y- spatial shifts that generate the maximum value in this convolution determine the 2D bead displacement of the bead from one frame to the next. To measure the motion orthogonal to the image plane (i.e. z-direction), we leverage the bead height-dependent radial changes in diffraction patterns that can be measured and calibrated to allow for nanometer-scale accuracy in the measurement of z-position. In all cases, the coverslip surface is simultaneously tracked using immobilized reference beads, allowing the absolute height of the beads with respect to the coverslip surface to be measured, and reducing the effects of noise from mechanical vibrations or thermal drift. Such measurements can be carried out in real time at 60 Hz for up to \approx 30 particles. These trajectories are then used to investigate and validate the dynamic force capabilities of the device.

A. Validation of Force Range

To validate our ability to apply controlled forces on small magnetic particles positioned at the sample plane, we employed two complementary approaches, as previously described^{12,21,22,24}. We note that force calibration methods can be challenging, particularly when the particle is near a bounding surface $^{25\text{--}27}.$ For small applied forces (typically $<20\,pN),$ we used a tethered bead assay in which single poly(ethylene glycol) molecules attach beads to the glass coverslip surface²⁸. A bead tethered by a polymer and pulled away from its anchoring point acts as a pendulum. The Brownian movement of the bead produces mean square fluctuations sensitive to the applied force via the equipartition theorem²⁹. By tracking the particle displacement and modeling the tracked motion using a Lorentzian function we extract the applied force^{28,30}. To a good approximation, the force on one-micron diameter MyOne C1 beads (Invitrogen 65801D) at z = 0.5 mm recovers the result calculated using the gaussmeter data (Fig. 3A), confirming that the magnetic field gradient provides a robust force profile at the sample plane. The values describing the response of the beads to a magnetic field were taken directly from the literature²³. For the MyOne (1 µm diameter), M-280 (2.8 µm diameter), and M-450 (4.5 µm diameter) beads, the volume susceptibility is measured as 1.38, 0.76 and 1.63, respectively, and the saturation magnetization is measured as 336, 336, and 353 kA m^{-1} , respectively²³.

A different approach is required at higher forces because the characteristic timescale of thermal bead fluctuations approaches the framerate of the camera and, at sufficiently high forces, the polymer tethers rupture. To achieve higher forces, we use larger 4.5 μ m diameter beads, which have a larger value of m_{sat} and a much larger volume, and thus experience hundreds of picoNewtons of force, and measure their motion using drag viscometry. Experimentally, beads are subjected

to constant force and their movements tracked over tens of microns to ensure that terminal velocity is achieved. From this bead motion data, and using the known drag coefficient, the drag force on the bead is extracted using Stoke's Law (Fig. 3B). Each data point represents an average over multiple magnetic beads. We find these large magnetic beads demonstrate bead-to-bead variation in force response, which we attribute to the variance in embedded paramagnetic material content. Nonetheless, the calculated values of force, which were determined using the measured magnetic field gradient and known value of the bead magnetic moment, are found to be in good agreement with measured values of average force. This provides confidence that the values of calibrated forces determined using the gaussmeter data are accurate and can be used in microrheological measurements to extract the mechanical response of the soft material surrounding the bead.

B. Application of Step Forces

Step function-like force behavior can be achieved by quickly rotating the magnet using the servo motor from one fixed position to another, thus creating an associated change in force on magnetic particles positioned in the sample plane (See Fig. 4). These rotational movements are small and occur internally, in comparison with the centimeter-scale translational movements needed in typical translational systems, and thus the magnet motion can be achieved over shorter timescales and with less noise, allowing tracking of the probe bead motion throughout the force application. Such movement is useful in active microrheology experiments where step-like force application is crucial for straightforward data analysis of a material's creep response⁶. The time delay to establish a new applied force is limited by the motor rotation speed, which in our design is on the order of 0.1 s.

Figure 4 demonstrates instrument's ability to quickly switch between arbitrary applied forces and to maintain tracking of the probe bead over long distances and times because the noise associated with magnet rotation is small and the illumination is uninterrupted by the rotary motion. At t = 0, a $4.5 \,\mu\text{m}$ bead is subjected to a step increase in force (regime A) and begins to move from the surface. In this regime, the bead speed is not constant due to the reduction in hydrodynamic drag as the bead-surface separation increases beyond a particle diameter³¹. At t = 5 s, the onset of Regime B, the magnet is rotated to the zero applied force position ($\phi = \pi/2$) and the bead motion immediately halts. Later at t = 15 s, the onset of Regime C, the magnet is returned to the original position, and the force is re-applied. At this bead-glass separation distance, the drag coefficient is constant and the bead approaches its terminal velocity. In contrast to prior NdFeB magnetic tweezer designs^{22,32}, our device can easily apply zero force to arrest bead motion, and can track bead motion while the magnets are being moved, allowing time-resolved measurement of bead dynamics during periods of force variation. Additionally, these high forces may be applied indefinitely without heating or sample degradation, which is a common problem in optical tweezers or electromagnet-based magnetic tweezers.

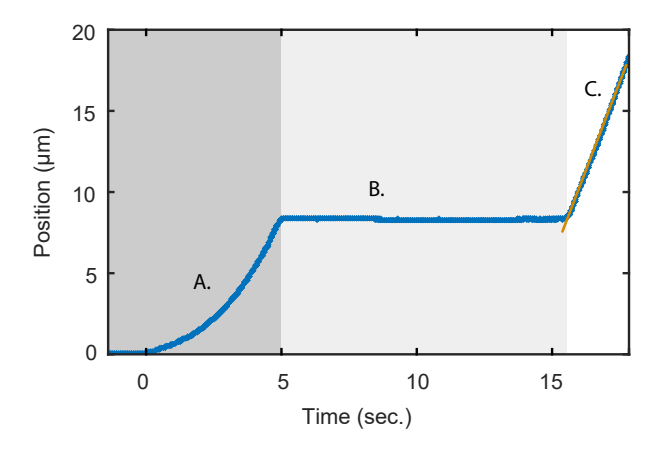


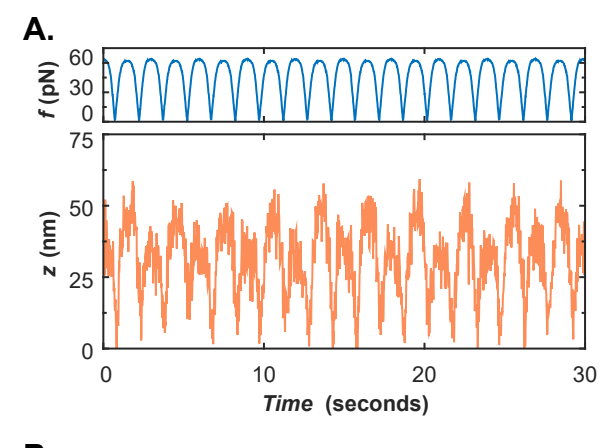
FIG. 4. Viscous drag experiment on a 4.5 µm bead in glycerol solution. As the bead moves from the surface, (A) the reduced hydrodynamic drag on the bead lessens and the bead velocity increases. (B) The magnet array is moved to the zero applied force position ($\phi = \pi/2$) and the bead motion immediately halts. (C) Later, force is re-applied and the bead approaches its terminal velocity. The dashed line (orange) represents the linear fit used to extract the terminal velocity and measure the applied force. Here, the applied force is 277 ± 0.76 pN, which is in good agreement with 271 pN, the estimate from measurements of the magnetic field gradient.

C. Application of Oscillatory Forces

Oscillatory forces are produced by continuously rotating the magnet assembly with respect to the fixed iron yoke. This causes a periodic variation in the field gradient at the sample, leading to periodic time-varying forces on beads in the sample plane. In practice, high frequency operation is limited by the speed at which images can be acquired and the speed at which the motor can rotate the magnet assembly, while low frequency operation is limited only by the time allowed for data capture.

Importantly, the addition of the oscillatory function does not compromise our ability to translate the magnet assembly orthogonal to the sample plane. Thus, by maintaining a constant angular magnet position, the device can be used in a completely analogous way to the standard operational mode of magnetic tweezers. The oscillatory function represents another dimension of control.

We note that the force-angle relationships presented in Fig. 3 demonstrate a force discontinuity at $\phi=\pm\pi/2$, where the superparamagnetic beads flip their polarization direction. Thus, although the instrument can robustly apply oscillations in force when the magnet orientation is continuously rotated, the form of the applied oscillatory behavior is not sinusoidal (Fig. 5). Although the application of non-sinusoidal forces by the instrument complicates the analysis of the measured behavior, there is a framework for interpreting and analyzing such non-sinusoidal data^{33–39}. We do not expect any measurable torque due to the flipping polarization direction based on the time scales we are able to access in this measurement. We capture images approximately every 10 ms, whereas we



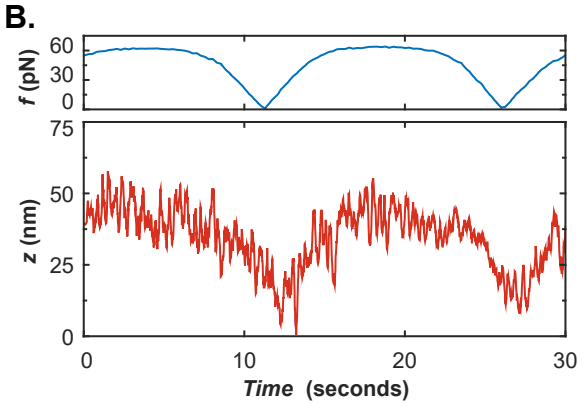


FIG. 5. Example traces of oscillatory data using a 4.5 µm bead in a polyacrylamide gel (3% acrylamide and 0.06% bis-acrylamide) at two frequencies. (A) The application of 0.67 Hz oscillatory force results in a nearly elastic response in the bead displacement. (B) 0.067 Hz oscillations in force also result in elastic response. We observe a slight variation in the loading during magnet rotation, in which the bead alternates between two maxima of slightly different values; this effect, which may arise from slight misalignment of the magnetic array, introduces a slight error in the measurement of the effective elastic constants. However, the uncertainty is relatively small ($\approx 10\%$ of mean) and the measured values are in good agreement with previously reported values.

expect the magnetic relaxation time constant to be $\approx 1 \,\mu\text{s}^{40}$.

To evaluate the ability of our instrument to accurately measure the dynamic mechanical response of elastic materials, we measure the motions of beads embedded in a polyacrylamide gel prepared with standardized protocols⁴¹ and subjected to oscillatory forces (Fig. 5). Experimentally, we measure the particle displacement as a function of time under applied force and determine the mean value of displacement or force using the maximal (peak) and minimal (troughs) values of the periodic traces. From the ratio of the mean values of the applied force and measured displacement, we calculate an effective spring constant, k, which provides a measure of the elastic energy stored by the gel network. In this loading geometry, the spring constant is equal to the elastic modulus scaled by a geometrical factor⁴²: $G' = \frac{k}{6\pi a}$. From these measurements, we estimate the elastic modulus of the gel to be 230 ± 22 Pa which is within a good approximation of bulk measurements

of 200 Pa^{43,44}. We find similar responses for two oscillation frequencies (0.67 Hz and 0.067 Hz), consistent with the expected insensitivity to frequency for elastic materials (Fig. 5).

IV. CONCLUSION

We have demonstrated a compact and versatile rotary NdFeB-based magnetic tweezers device that can achieve rapid force switching and can produce oscillatory forces through a wide range of frequencies (≈0.01 Hz to 1 Hz) and applied forces (≈0 pN to 1000 pN). In comparison with other methods which probe micromechanical behavior, this instrumental design presents several advantages including relatively simple and compact layout, stable zero force behavior, and multiple modes of operation, without compromising the typical advantages of NdFeB-based magnetic tweezers including multiplexing. Similar designs could be employed in a portable and modular fashion on microscopes not explicitly designed for magnetic tweezers work, enabling the coupled use of micromechanical measurements with a wider range of characterization techniques.

V. ACKNOWLEDGEMENTS

This work was partially supported by the National Science Foundation (NSF) Grant DMR-2004937. We thank Skip Mahn, Kevin McClune, Daniel Pavich, Jose Perez, David Tam, and the UC Santa Barbara Mechanical Engineering Capstone Program and staff who contributed to the initial efforts. We thank Greg Dahlen, Trevor Marks and David Bothman for helpful conversations and the UCSB College of Engineering machine shop for assistance in fabrication of the device. JB acknowledges support from the NSF MRSEC DMR-2011846.

VI. DATA AVAILABILITY STATEMENT

The data that support the findings of this study are available from the corresponding author upon reasonable request.

- ¹C. D. Chapman and R. M. Robertson-Anderson, Physical review letters 113, 098303 (2014).
- ²V. Y. Rudyak, A. Minakov, and M. Pryazhnikov, Journal of Molecular Liquids 329, 115517 (2021).
- ³S. Paladugu, S. Kaur, G. Mohiuddin, R. K. Pujala, S. K. Pal, and S. Dhara, Soft Matter **16**, 7556 (2020).
- ⁴A. Habibi, C. Blanc, N. B. Mbarek, and T. Soltani, Journal of Molecular Liquids 288, 111027 (2019).
- ⁵F. G. Schmidt, F. Ziemann, and E. Sackmann, European biophysics journal **24**, 348 (1996).
- ⁶A. R. Bausch, W. Möller, and E. Sackmann, Biophysical journal **76**, 573 (1999).

- ⁷D. T. Chen, Q. Wen, P. A. Janmey, J. C. Crocker, and A. G. Yodh, Annu. Rev. Condens. Matter Phys. **1**, 301 (2010).
- ⁸M. L. Gardel, M. T. Valentine, and D. A. Weitz, in *Microscale diagnostic techniques* (Springer, 2005) pp. 1–49.
- ⁹T. A. Waigh, Reports on Progress in Physics **68**, 685 (2005).
- ¹⁰Y. Seol and K. C. Neuman, in *Single Molecule Analysis* (Springer, 2018) pp. 297–316.
- ¹¹ Y. Yang, J. Lin, R. Meschewski, E. Watson, and M. T. Valentine, BioTechniques 51, 29 (2011).
- ¹²N. Ribeck and O. A. Saleh, Review of Scientific Instruments 79, 094301 (2008)
- ¹³B. M. Lansdorp, S. J. Tabrizi, A. Dittmore, and O. A. Saleh, Review of Scientific Instruments 84, 044301 (2013).
- ¹⁴A. Huhle, D. Klaue, H. Brutzer, P. Daldrop, S. Joo, O. Otto, U. F. Keyser, and R. Seidel, Nature communications 6, 1 (2015).
- 15C. Jiang, T. A. Lionberger, D. M. Wiener, and E. Meyhofer, Review of Scientific Instruments 87, 084304 (2016).
- ¹⁶J. G. Piccolo, J. Méndez Harper, D. McCalla, W. Xu, S. Miller, J. Doan, D. Kovari, D. Dunlap, and L. Finzi, Journal of Applied Physics 130, 134702 (2021).
- ¹⁷F. Amblard, B. Yurke, A. Pargellis, and S. Leibler, Review of Scientific Instruments 67, 818 (1996).
- ¹⁸N. A. Zacchia and M. T. Valentine, Review of Scientific Instruments 86, 053704 (2015).
- ¹⁹J. Lipfert, X. Hao, and N. H. Dekker, Biophysical Journal **96**, 5040 (2009).
- ²⁰T. Strick, J.-F. Allemand, D. Bensimon, and V. Croquette, Biophysical journal 74, 2016 (1998).
- ²¹C. Gosse and V. Croquette, Biophysical journal **82**, 3314 (2002).
- ²²J. Lin and M. T. Valentine, Review of Scientific Instruments 83, 053905 (2012)
- ²³G. Fonnum, C. Johansson, A. Molteberg, S. Mørup, and E. Aksnes, Journal of Magnetism and Magnetic Materials 293, 41 (2005).
- ²⁴K. C. Neuman and A. Nagy, Nature methods **5**, 491 (2008).
- ²⁵Z. Yu, D. Dulin, J. Cnossen, M. Köber, M. M. van Oene, O. Ordu, B. A. Berghuis, T. Hensgens, J. Lipfert, and N. H. Dekker, Review of Scientific Instruments 85, 123114 (2014).
- ²⁶S. N. Innes-Gold, I. L. Morgan, and O. A. Saleh, The Journal of Chemical Physics **148**, 123314 (2018).
- ²⁷J. W. Swan and E. M. Furst, Biophysical journal **104**, 863 (2013).
- ²⁸A. Dittmore, D. B. McIntosh, S. Halliday, and O. A. Saleh, Physical review letters 107, 148301 (2011).
- ²⁹I. L. Morgan and O. A. Saleh, PloS one **16**, e0262028 (2021).
- ³⁰T. Strick, J. Allemand, D. Bensimon, A. Bensimon, and V. Croquette, Science 271, 1835 (1996).
- ³¹H. Faxén, Annalen der Physik **373**, 89 (1922).
- ³²J. Lin and M. T. Valentine, Applied Physics Letters **100**, 201902 (2012).
- ³³R. H. Ewoldt, Journal of Rheology **57**, 177 (2013).
- ³⁴K. Hyun and M. Wilhelm, Macromolecules **42**, 411 (2009).
- ³⁵ K. Hyun, M. Wilhelm, C. O. Klein, K. S. Cho, J. G. Nam, K. H. Ahn, S. J. Lee, R. H. Ewoldt, and G. H. McKinley, Progress in Polymer Science 36, 1697 (2011).
- ³⁶S. A. Rogers, J. D. Park, and C.-W. J. Lee, Rheologica Acta **58**, 539 (2019).
- ³⁷S. A. Rogers, Journal of Rheology **56**, 1129 (2012).
- ³⁸J. Kim, D. Merger, M. Wilhelm, and M. E. Helgeson, Journal of Rheology 58, 1359 (2014).
- ³⁹H. S. Joyner, Annual review of food science and technology **12**, 591 (2021).
- ⁴⁰P. P. Liu, K. Skucha, Y. Duan, M. Megens, J. Kim, I. I. Izyumin, S. Gambini, and B. Boser, IEEE journal of solid-state circuits 47, 1056 (2012).
- ⁴¹Y. Aratyn-Schaus, P. W. Oakes, J. Stricker, S. P. Winter, and M. L. Gardel, JoVE (Journal of Visualized Experiments), e2173 (2010).
- ⁴²F. Ziemann, J. Rädler, and E. Sackmann, Biophysical Journal **66**, 2210 (1994).
- ⁴³M. Funaki and P. A. Janmey, Biology and Engineering of Stem Cell Niches , 363 (2017).
- ⁴⁴L. Vincent and A. Engler, Comprehensive biomaterials. Elsevier Press, New York, 51 (2011).